ResearchGate

See discussions, stats, and author profiles for this publication at: https://www.researchgate.net/publication/305803582

Ru–TiO2 semiconducting nanoparticles for the photo-catalytic degradation of bromothymol blue

Article *in* Journal of Materials Science Materials in Electronics · August 2016

DOI: 10.1007/s10854-016-5449-6

CITATIONS
0

READS
46

6 authors, including:

Raviraj Kulkarni
Gogte Institute of Technology
53 PUBLICATIONS **232** CITATIONS
SEE PROFILE

Ramesh Malladi
B.L.D.E.A's Dr P.G.H. College of Engineering…
10 PUBLICATIONS **11** CITATIONS
SEE PROFILE

Manjunath S Hanagadakar
Hirasugar Institute of Technology ,Nidasos…
7 PUBLICATIONS **11** CITATIONS
SEE PROFILE

Mrityunjay Doddamani
National Institute of Technology Karnataka
40 PUBLICATIONS **23** CITATIONS
SEE PROFILE

All in-text references underlined in blue are linked to publications on ResearchGate, letting you access and read them immediately.

Available from: Mrityunjay Doddamani
Retrieved on: 16 September 2016

J Mater Sci: Mater Electron
DOI 10.1007/s10854-016-5449-6

Ru–TiO_2 semiconducting nanoparticles for the photo-catalytic degradation of bromothymol blue

R. M. Kulkarni[1] · R. S. Malladi[1] · M. S. Hanagadakar[1] · M. R. Doddamani[2] · B. Santhakumari[3] · S. D. Kulkarni[4]

Received: 6 June 2016 / Accepted: 25 July 2016
© Springer Science+Business Media New York 2016

Abstract Photo-catalytic degradation of bromothymol blue (BTB) in an aqueous medium by Ru–TiO_2 using UVC (254 nm) irradiation was investigated for a pH range of 4.0–8.0. The liquid impregnation method was used to synthesize 0.2, 0.4 and 0.8 % ruthenium doped TiO_2 (Ru–TiO_2) nanoparticles. The characterizations of resulting nanoparticles were done using X-ray diffraction, scanning electron microscopy, fourier transform infrared spectroscopy, transmission electron microscopy (TEM) and energy dispersive X-ray spectroscopy analysis. The crystallite sizes of doped and undoped nanoparticles were determined from X-ray diffraction spectra using Scherrer equation. The average crystallite size of undoped TiO_2 was found to be 17.00 nm, whereas the crystallite sizes of 0.2, 0.4 and 0.8 % Ru–TiO_2 were 16.67, 15.70 and 14.40 nm respectively. The TEM images confirm the particle sizes to be 10–40 nm. Pseudo-first order rate constants (k_{obs}) determined were found to decrease with increase in pH. The effect of BTB Concentration, catalyst dosage, a percentage of doping of photo catalyst, pH and UV light intensity of BTB on the degradation rate were also examined.

✉ R. M. Kulkarni
ravirajmk@git.edu

[1] Department of Chemistry, KLS Gogte Institute of Technology (Autonomous) Affiliated to Visvesvaraya Technological University, Belagavi, Karnataka 590 008, India

[2] Mechanical Engineering, National Institute of Technology Karnataka, Surathkal, India

[3] Center for Materials Characterization Division, CSIR-National Chemical Laboratory, Pune, Maharashtra 411008, India

[4] Department of Atomic and Molecular Physics, MIT Campus, Manipal University, Manipal 576104, India

1 Introduction

A wide variety of organic contaminants has been detected in the aquatic environment which are discharged through municipal waste-water, industrial effluents, commercial operations, runoff from agricultural lands, chemical spills etc [1]. Till now, the conventional and biological methods have not been able to get rid of these persistent organic contaminants from the environment [2].

Dye effluent generated from textile and dye industries has to be treated due to its impact on flora and fauna and growing public concern over the toxicity and carcinogenicity [3–5]. This fact compels elimination of dyes in the effluent treatment plants [6].

Advanced oxidation processes (AOPs) have been used extensively for the degradation of harmful organic contaminants [7], which are resistant to biological and conventional treatment methods. AOPs depend on the generation of highly reactive radical species such as $OH^{\cdot}$ by chemical or photochemical methods, which decomposes a number of organic contaminants without being selective [8–10]. The technique primarily focuses on the usage of semiconductor particles activated by UV or visible light for degradation of environmental contaminants yielding to partial or complete mineralization of the organic contaminants [11, 12].

Metal oxide semiconductor Titanium dioxide (TiO_2) nanoparticles have attracted much interest due to their low cost, greater efficiency and stability [13, 14]. It allows UV light to excite the valence electrons as it has a band gap of 3.2 eV [15], the valance electrons jump into the conduction

Published online: 02 August 2016

band generating positive holes in the valance band [16]. The efficacy of the photo catalyst depends on the rate of electron–hole recombination in TiO_2 [17, 18]. This rate of recombination can be minimized by doping the TiO_2 with metals such as silver, ruthenium, copper, iron, chromium, nickel etc [19–21].

These doped cations reduce the band gap and shift the threshold for photonic excitation of the TiO_2 towards the visible range [22]. Ruthenium might act as a suitable element for doping of TiO_2, because of its closeness in atomic radius with TiO_2 (Ru—0.056 nm, Ti—0.060 nm) [23].

The model compound used for study bromothymol blue (BTB) is a textile dye derivative. The photo-catalytic degradation of bromothymol blue by TiO_2 has been investigated earlier [24]. From the application point of view, kinetics of degradation of textile dye derivatives by doped nanostructure is essential. Therefore, in the present work, we have undertaken a detailed study on the photo-catalytic degradation of bromothymol blue by prepared Ru–TiO_2 nanoparticles in an aqueous medium by varying reaction parameters namely pH of the reaction, substrate concentration, catalyst concentration, percentage of doping of photo-catalyst and intensity of UV-light.

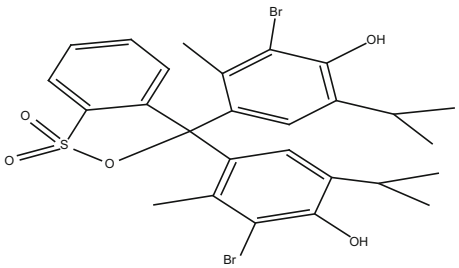

Chemical structure of Bromothymol blue (BTB) $C_{27}H_{23}Br_2O_5S$

2 Materials and methods

2.1 Reagents and chemicals

A stock solution of bromothymol blue (Sigma-Aldrich) was prepared by dissolving appropriate amount of sample in double distilled water. The TiO_2 (anatase) (SRL) and $RuCl_3{\cdot}3H_2O$ (SRL) samples were directly used to prepare Ru doped TiO_2 without any further purification. The chemicals and reagents used to carry out the degradation study were of analytical grade.

2.1.1 Instruments used

1. For kinetic measurements, a CARY 50 Bio UV–Vis Spectrophotometer (Varian BV, The Netherlands) with a temperature controller and HPLC system (Agilent 1100 series, USA) were used.
2. For degradation study, a mercury lamp (PHILIPS, TUV 8W T5, $E_{max} = 254$ nm) mounted inside the UV cabinet was used. The typical light intensity illuminated on the surface of the reaction mixture was 4 mW cm^{-2}.
3. For intensity measurement an optical power meter (Newport 2936—C) and for pH measurements, Elico pH meter models LI 120 were used.
4. For characterization of nanoparticles, a Siemens X-ray Diffractometer (Cu source) (XRD) AXS D5005 was used to identify the particle size of the doped TiO_2. The surface morphology was studied using a Scanning electron microscope (SEM) JEOL JSM 6360.
5. FTIR Perkin Elmer model-spectrum 100 was used for the characterization.
6. The topography and particle size of Ru-doped TiO_2 were measured using JEOL JEM-2010 transmission electron microscopy (TEM). Before the analysis, the catalyst sample ultrasonically dispersed in a solvent and dropped on a copper grid. The sample was allowed to dry before TEM analysis.

2.2 Photo-catalyst preparation

Ruthenium (Ru) doped anatase TiO_2 nanoparticles were prepared by liquid impregnation method. For ruthenium doping, 0.2, 0.4 and 0.8 % (mole ratio) of $RuCl_3{\cdot}3H_2O$ was dissolved in 100 ml of 0.2 M HCl solution. Further, 1.0 g of Anatase nanoparticles TiO_2 was added to the solution. The resultant slurry was thoroughly stirred for 3 h and allowed to settle at room temperature for 24 h. Afterward, the slurry was dried out in an oven at 80 °C for further 24 h. The dried solids were ground in a mortar and calcined at 400 °C for 3 h in a muffle furnace because the Anatase to Rutile phase transformation takes place above 400 °C [25, 26].

2.3 The photo-catalysis process

To investigate the photo-catalytic degradation, a known concentration of BTB solution and the buffer was taken in a Pyrex beaker, and then a dosage of 100 mg l^{-1} Ru–TiO_2 nanoparticles was added. Before illumination, the suspensions were stirred at a dark place for 1 h to reach adsorption and desorption equilibrium between the BTB and photo-catalyst. Then, the beaker was placed in a photo-catalytic chamber under 8W UV-lamp (Phillips) with a wavelength peak at 254 nm with continuous stirring for adsorption–desorption equilibrium and then exposed to UV light. At the interval of every 15 min, the solution was

taken out and centrifuged at 5000 rpm for 10 min. The decrease in the concentration of bromothymol blue was monitored at 429 nm ($\varepsilon = 10{,}860\ l\ M^{-1}\ cm^{-1}$) using UV–Vis spectrophotometer (Varian CARY 50 Bio UV–Vis Spectrophotometer).

3 Results and discussion

3.1 Comparison of different photo-catalysts

The rate of photo-catalytic degradation of BTB with UV, UV/TiO_2, UV/0.2 % Ru–TiO_2, UV/0.4 % Ru–TiO_2 and UV/0.8 % Ru–TiO_2 was studied. It was observed that the degradation effect of BTB treatment with UV/Ru–TiO_2 was more efficient than other two treatments namely UV and UV/TiO_2 (Fig. 1).

Effect of ruthenium doping on anatase TiO_2 was studied by varying the percentage of ruthenium from 0.2 to 0.8 % (mole ratio) an increase in the content of ruthenium leads to decrease in the particle size and increase in the photo-catalytic activity [27] as shown in Fig. 1. Smaller particle size increases surface area and higher content ruthenium may also favour separating charge carriers efficiently, inhibiting the recombination of electron–hole pairs, and thus increase the photo-catalytic activity [28]. The photo-catalytic degradation rate was highest with 0.8 % Ru–TiO_2; hence, further studies were carried out with 0.8 % Ru–TiO_2. Increasing the percentage of ruthenium above 0.8 % resulted in the deposition of ruthenium on the surface of the TiO_2 but not in the crystal lattice.

The % degradation efficiency of BTB was studied under same conditions with UV, UV/TiO_2, UV/0.2 % Ru–TiO_2, UV/0.4 % Ru–TiO_2, UV/0.8 % Ru–TiO_2 and percentage adsorption in dark was also determined. The percentage degradation efficiency of BTB was found to be 48, 60, 75, 82 and 95 % with UV, UV/TiO_2, UV/0.2 % Ru–TiO_2, UV/0.4 % Ru–TiO_2 and UV/0.8 % Ru–TiO_2 respectively within 100 min as shown in Fig. 2. The % degradation efficiency of UV/0.8 % Ru–TiO_2 is about 35 % higher than UV/TiO_2 report by Haque et al. under our experimental conditions with [Photocatalyst] = 100 mg l^{-1}, [BTB] = 5×10^{-5} mol dm^{-3} at pH 4 and light intensity 4 mW cm^{-2}.

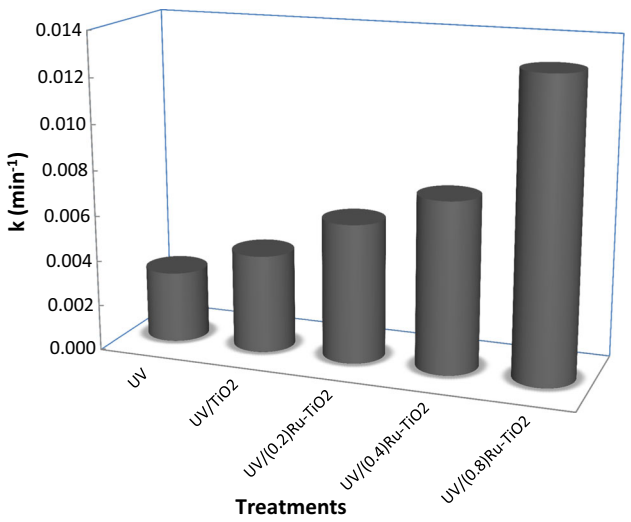

Fig. 1 Rate constants for the photo catalytic degradation of BTB by various treatments

3.2 Characterization of TiO_2 and Ruthenium doped TiO_2

3.2.1 X-ray diffraction studies (XRD)

X-ray diffraction pattern of pure TiO_2 and Ru–TiO_2 were obtained from an X-ray diffractometer using Cu K_α radiation over a scan range of 2θ (10°–90°). XRD patterns of pure and 0.2, 0.4 and 0.8 % Ru–TiO_2 were shown in Fig. 3. Several well defined diffraction reflections were appeared in the pattern 25.2, 38.0, 48.2, 53.9, 55.0, 62.5, 70.2, 70.8, and 78.5, 82.9, which corresponds to the XRD pattern of all the ten peaks of anatase TiO_2 with lattice planes of (101), (004), (200), (105), (211), (204), (116), (220), and (215), (224), respectively. The absence of metal peaks is due to the ultrafine dispersion of TiO_2 nanoparticles and or due to very low metal concentration. The average particle sizes of prepared nanoparticles were determined from a full width half maximum of A (101) peak of anatase TiO_2 by applying Scherrer Eq. (1) [29]

$$D = \frac{k\lambda}{\beta\cos\theta} \tag{1}$$

where k is a constantly called shape factor is equal to 0.94, λ is the X-ray wavelength is equal 0.154 nm, β, is the full width at half maximum and θ is the half diffraction angle.

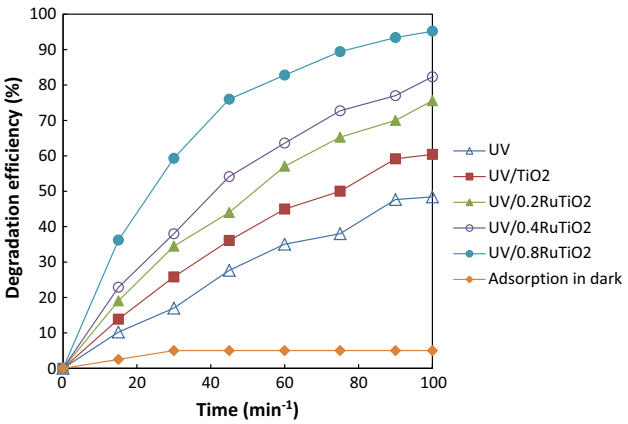

Fig. 2 % degradation efficiencies of various treatment methods with time

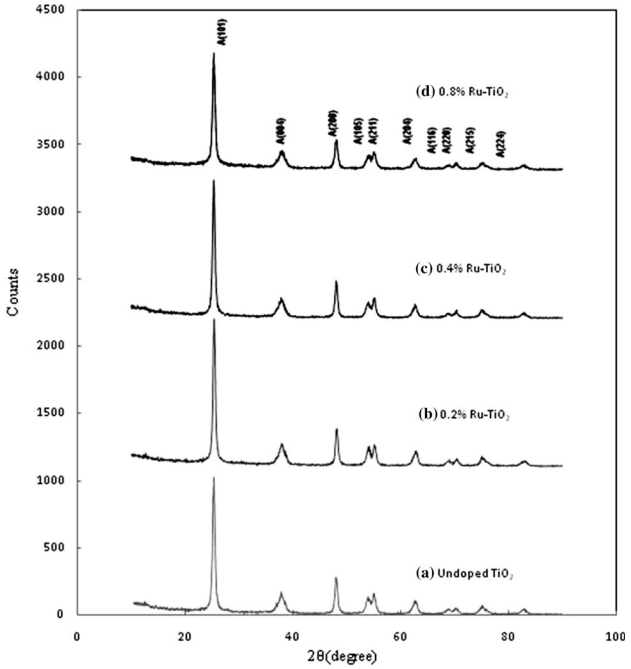

Fig. 3 X-ray diffraction patterns of **a** undoped TiO_2, **b** 0.2 % Ru–TiO_2, **c** 0.4 % Ru–TiO_2, **d** 0.8 % Ru–TiO_2

The average particle size of TiO_2, 0.2 % Ru–TiO_2, 0.4 % Ru–TiO_2, 0.8 % Ru–TiO_2 were found to be 17.00, 16.67, 15. 70 and 14.40 nm respectively.

3.2.2 Scanning electron microscope

The SEM images of undoped and Ru-doped TiO_2 nanoparticles obtained at the high magnification 15000× using JEOL JSM-6360 are presented in Fig. 4a, b. Thin films of the sample were prepared on a carbon coated copper grid by just dropping a very small amount of the sample on the grid, extra solution was removed using a blotting paper and then the film on the SEM grid were allowed to dry by putting it under a mercury lamp for 5 min which reveal that synthesized nanoparticles possess a porous and spongy network of unequal shapes resulting in the high surface area. SEM images show that ruthenium is not equally deposited on the surface of TiO_2 nanoparticles; this is in agreement with the earlier literature [12].

3.2.3 Energy dispersive X-ray spectroscopy

The EDX pattern of Ru–TiO_2 (Fig. 5) was obtained using the JEOL JED-2300 equipment. The EDX shows the presence of three different X-ray patterns linked with O Kα, Ru Kα, and Ti Kα [30]. The peaks from the spectrum reveal the presence of Ti, O and Ru at 4.508, 0.525 and 2.558 keV respectively. The atomic % of Ti, O and Ru is 36.40, 62.79 and 0.81 respectively. This composition of Ti,

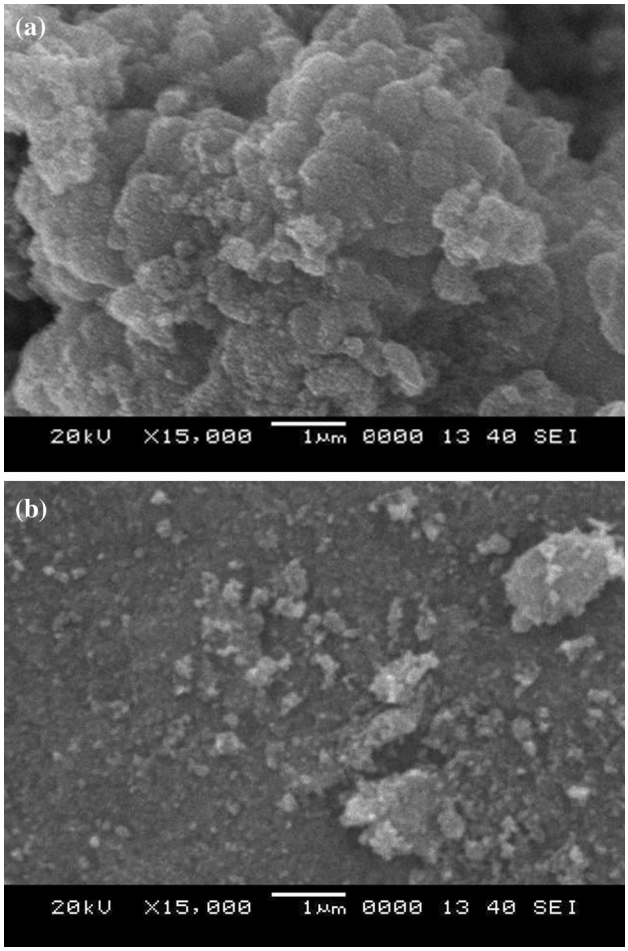

Fig. 4 SEM micrographs of **a** undoped TiO_2, **b** 0.8 % Ru–TiO_2 nano particles

O and trace amount of Ru revealed that the formation of non-stoichiometric TiO_2 with oxygen vacancy, which leads to better photo-catalytic activity [31].

3.2.4 Transmission electron microscope

A typical TEM image of Ru–TiO_2 powders synthesized by Liquid Impregration method is presented in Fig. 6a, b, which reveals that the synthesized Ru–TiO_2 nanoparticles is well crystallized uniformly dispersed aggregates having the spherical rod in shape without defects. The average particle size of the nanoparticles was found to be 15-20 nm. These results are in good agreement with that of calculated particle size by Scherrer equation. The selected area electron diffraction pattern (SAED) is shown in inset of Fig. 6b. The D values of diffractions were obtained from the rings which can be assigned [101], [004], [200], and [211] (Table 1) and these values are in agreement with the D values obtained from XRD. In SAED, the small spots making up rings, each spot arising from Bragg reflection from an individual crystallite indicates our sample is poly-

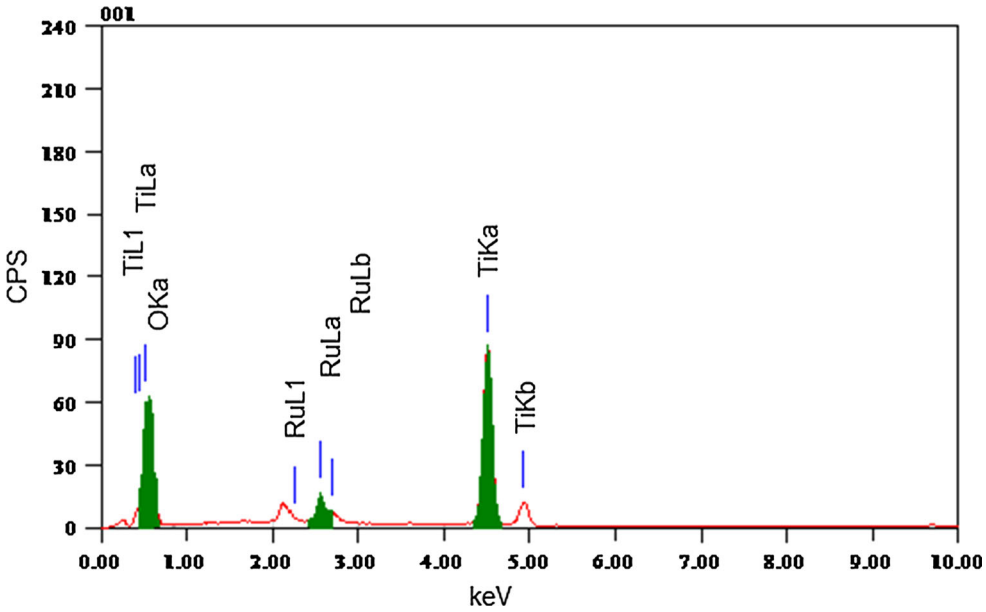

Fig. 5 EDX analysis of 0.8 % Ru/TiO_2

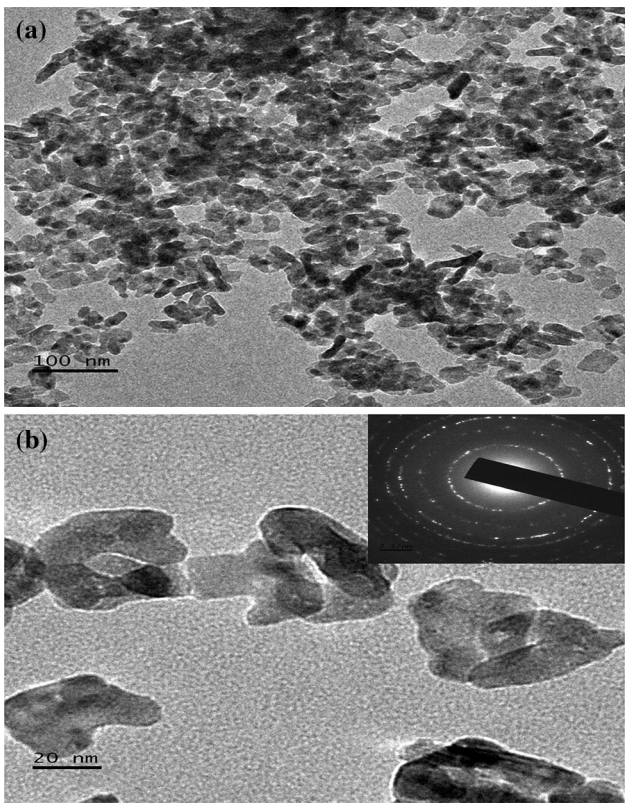

Fig. 6 TEM micrographs of 0.8 % Ru/TiO_2 at **a** 100 nm resolution and **b** 20 nm resolution (*inset* SAED pattern)

nano-crystalline in nature. In poly-nano-crystalline samples, if more than one crystal contributes to the selected area diffraction pattern, it can be difficult or impossible to analyze. SAED is similar to XRD but unique in that areas as small as several hundred nanometers in size can be examined, whereas XRD typically samples areas several centimetres in size due to that we could observe small difference in the D values of SAED and XRD [32, 33].

3.2.5 Fourier transform infrared (FTIR) spectra analysis

The FT-IR spectra of pure TiO_2 and $Ru–TiO_2$ nanoparticles were shown in Fig. 7. The FT-IR spectra of TiO_2 and $Ru–TiO_2$ show a broad band between 3500–3000 cm^{-1}, which is a characteristic band of associated hydroxyl groups. The other peaks at 1635 cm^{-1} correspond to the stretching vibration of a hydroxyl group and representing the water as moisture [34]. The peak observed between 750 and 500 cm^{-1} indicates the Ti–O stretching bands. Calcination of TiO_2 and $Ru–TiO_2$ sample at 600 °C leaves a strong band between 800 and 450 cm^{-1}, which can be attributed to the formed of TiO_2 nanoparticles [35].

3.2.6 Band gap measurement

The bandgap measurements of nanoparticles were made from the diffuse reflectance spectra collected using a Perkin Elmer Lambda 950 UV/Vis/NIR spectrophotometer with a 150 mm integrating sphere attachment. Diffuse reflectance measurements were made between 800 and 200 nm using $BaSO_4$ as a reflectance standard. The optical bandgaps (Eg) of the nanoparticles were determined from the Tauc plot of the Kulbelka–Munk function obtained from the diffuse reflectance spectra. The Kulbelka–Munk function is given by the equation $F(R) = (1 - R)^2/2R$, where R is the diffuse reflectance of the sample. Extrapolation of the linear portion of the modified Kubelka–Munk function, $[F(R)h\upsilon]^{1/2}$ vs the photon energy ($h\upsilon$) curve on the zero ordinate gives the Eg (Fig. 8). The band gap of

Table 1 Selected area electron diffraction data

2R [1/nm]	R [1/nm]	SAED D [nm]	XRD D [nm]	Difference SAED and XRD	D [A^0]	h k l	2-theta
5.92	2.96	0.3378	0.3496	0.0118	3.38	101	25.45
8.87	4.43	0.2254	0.2352	0.0098	2.25	004	38.22
10.6	5.30	0.1886	0.1882	0.0004	1.89	200	48.28
12.6	6.30	0.1587	0.1667	0.0080	1.59	201	55.00

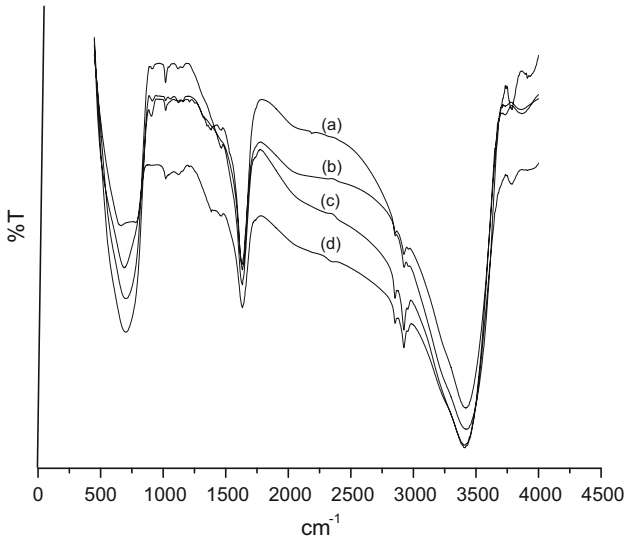

Fig. 7 FT-IR spectra of **a** pure TiO_2, **b** 0.2 % Ru–TiO_2, **c** 0.4 % Ru–TiO_2, **d** 0.8 % Ru–TiO_2 nanoparticles

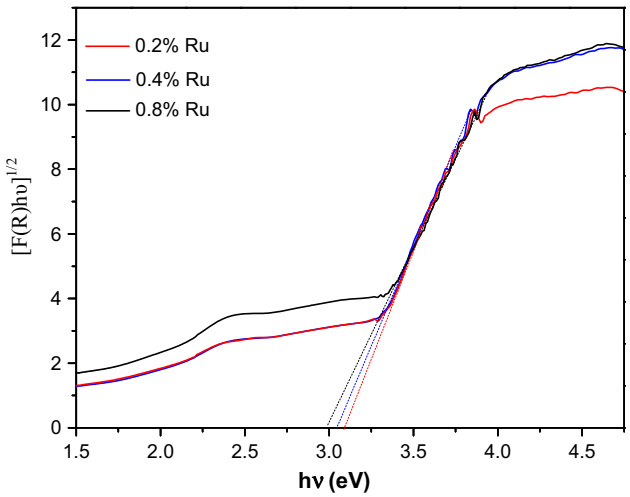

Fig. 8 Plot of $[F(R)h\upsilon]^{1/2}$ versus the photon energy ($h\upsilon$)

0.2, 0.4 and 0.8 % Ru–TiO_2 was found to be 3.10, 3.04 and 2.96 eV respectively. However, in the literature it is reported that the pure anatase TiO_2 nanoparticles shows the band gap 3.2 eV. This red shift is due to the localized energy level introduced by the Ru in the forbidden energy range of TiO_2 [36]. From the decrease in the value of band gap it is confirmed that ruthenium is successfully doped in TiO_2 lattice [31].

3.2.7 Surface area measurement

Photo-catalytic activity of Ru-doped TiO_2 also depends on the surface area of the particles. Hence, it would be interesting to determine the surface area of Ru-doped TiO_2 nanoparticles. The specific surface area of the nanoparticles was measured by the BET nitrogen gas adsorption method using Smart Instruments Surface Area Analyser (Smart-Sorb 92/93).

Our studies indicate that synthesized nanoparticles showed a surface area of 85.23, 88.79, 92.91 and 94.28 m^2/g for pure TiO_2, 0.2 % Ru–TiO_2, 0.4 % Ru–TiO_2 and 0.8 % Ru–TiO_2 nanoparticles respectively. The decrease in particle size can be explained on the basis of Nae-Lih Wu's theory [37]. According to Nae-Lih Wu's theory, the motion of the crystallites is restricted due to the interaction on the boundaries between TiO_2 and Ru [38–40], which results in the reduction of particle size of TiO_2. Hence, the specific surface area increases with decrease in particle size. The very high surface area of 0.8 % Ru–TiO_2 nanoparticles is responsible for the enhanced photo-catalytic degradation of BTB.

3.3 Variation of BTB concentration

The effect of initial of dye concentration on the rate of photo-catalytic degradation of bromothymol blue at pH 4 was studied at different concentrations varying from 2.0–20.0 $\times$ 10^{-5} mol dm^{-3}. Initially, the rate constant, k_{obs}, was found to increase with the increase in substrate concentration from 2.0–12.0 $\times$ 10^{-5} mol dm^{-3}. A further increase in BTB concentration above 12.0 $\times$ 10^{-5} mol dm^{-1} resulted in a decrease in the rate constant (Fig. 9). This trend can be attributed to the fact that as initial concentrations of the dye increase, the colour of the irradiating mixture progressively becomes intense which prevents the penetration of light photons to reach the surface of the catalyst. Hence, the generation of a relative amount of $OH^{\cdot}$ and $O_2^{\cdot-}$ on the surface of a catalyst does not

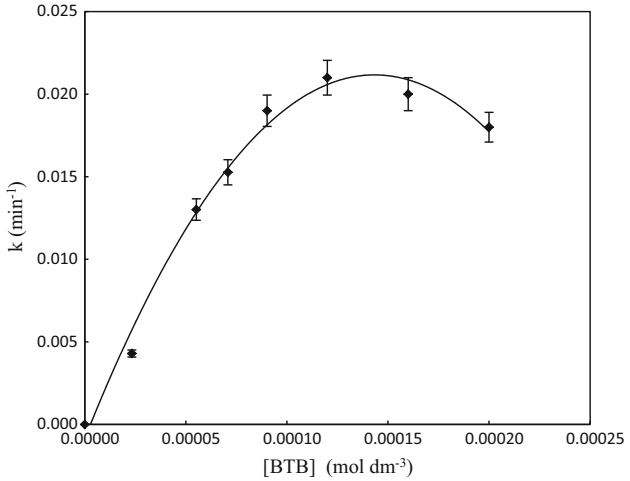

Fig. 9 Effect of variation of [BTB] on the degradation of BTB by Ru–TiO_2 at 25 °C. [Ru–TiO_2] = 100 mg l^{-1} pH = 4.0

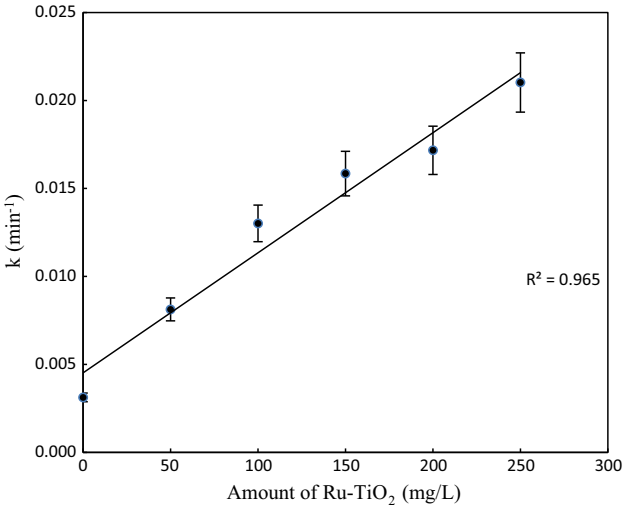

Fig. 10 Effect of variation of Ru–TiO_2 dosage on the degradation of BTB at [BTB] = 5.0 × 10^{-5} mol dm^{-3}

increase, as the intensity of the light and the irradiation time are constant. Consequently, the rate of photo-catalytic degradation decreases with increase in a concentration of BTB [24].

3.4 Effect of catalyst dosage

The effect variation in the photo-catalyst dosage on the degradation kinetics of bromothymol blue was studied using a different concentration of 0.8 % Ru–TiO_2 varying from 0–250 mg dm^{-3} and keeping other conditions constant. The rate constant, k_{obs}, was found to increase with an increase in the dosage of a catalyst as shown in Fig. 10. This can be attributed to the fact that, as the dosage of Ru–TiO_2 increases, the exposed surface area of the photo-catalyst also increases. The results are in agreement with the earlier reports [24, 41, 42].

3.5 Adsorption experiment

The adsorption experiment was carried by varying the BTB concentration from 2.0–20 × 10^{-5} mol dm^{-3}. The appropriate amount of BTB solution was taken in 100 ml beaker and 10 mg of Ru–TiO_2 nano particles was added. The pH value of the each set was adjusted to 4, 5, 6, 7 and 8 respectively. The solution was sealed and stirred at 25 °C for overnight in the absence of UV light. The solution was centrifuged and the BTB concentration of the supernatant was measured by UV spectrophotometer. The adsorption amount (Capacity) was calculated using the following equation (Table 2).

$$S = \frac{(C_0 - C)V}{m}$$

where S basically represents efficiency of adsorption (mol g^{-1}), C_0 is the initial concentration of BTB, C is the BTB is the equilibrium concentration (mol dm^{-3}), V is the volume (dm^3) of the solution, and m is the mass of added Ru–TiO_2 (g).

The adsorption of the BTB on the surface of Ru–TiO_2 photo-catalyst was studied by continuous stirring the aqueous solution of BTB in the dark for 24 h in a flask containing varying amounts of Ru–TiO_2. The analysis of BTB concentration after centrifugation shows no observable loss of the dye. Hence, adsorption has no significant effect on the degradation rate.

3.6 Effect of pH

pH is an important parameter in photo-catalytic reactions, it gives information pertaining to the surface properties of the photo-catalyst and adsorption behaviour of pollutants. Effect of pH on the degradation of BTB in water medium of Ru–TiO_2 was studied between pH 4.0–8.0 under UV-light. Whilst maintaining other reaction conditions constant. The photo-catalytic degradation of BTB was higher

Table 2 Adsorption capacities at different pH, [BTB] = 5 × 10^{-5}, (0.8 %) Ru–TiO_2 = 100 mg l^{-1}

Sl. No	pH	Adsorption capacity (mol g^{-1})
1	4	0.00091
2	5	0.00083
3	6	0.00074
4	7	0.00067
5	8	0.00060

in the pH range 4.0–6.0 and slightly lower in the pH range 7.0–8.0 as shown in Fig. 11. This performance possibly elucidated on the bases that increase in the rate of photo-catalytic degradation was due to the surface activity of photo-catalyst. The adsorption at pH 4.0–6.0 is favoured by attractive electrostatic forces existing between BTB anion and as Ru–$TiOH_2^+$, where Ru–$TiOH_2^+$ is a major active species in this pH range. Where as in basic medium, i.e. pH 7.0–8.0 Ru–TiO^- is a major active species, Hence electrostatic repulsion between two negatively charged species, Ru–TiO^- and BTB anion disfavours photo-catalytic degradation [43, 44]. The adsorption capacity decreases with increase in the pH from 4.0 to 8.0. The BTB react with the H^+ and OH^- in solution to form two different BTB species viz., BTB° (neutral) and $BT\bar{B}$ (anion). The proportion of BTB in different forms can be calculated from the pK_a (7.1) [45] as shown in Fig. 12. BTB neutral species dominates in the pH range 4.0–7.0 and are adsorbed at a higher degree than highly ionised species. Whereas BTB^- dominates in the pH range above 7.0 and are less adsorbed due to electrostatic repulsion forces. Whereas above pH 7 the adsorption of BTB neutral is due to weak van der Waals forces of attraction. This observation is in line with the earlier report [46].

3.7 Effect of UV lamp distance

The variation of UV light intensity on the rate constant of photo-catalytic degradation of BTB was studied by altering the distance of UV lamp from the reaction mixture as shown in Fig. 13. It is observed that the rate constant increased with increase in the light intensity. This can be attributed due to the fact that as the intensity of light

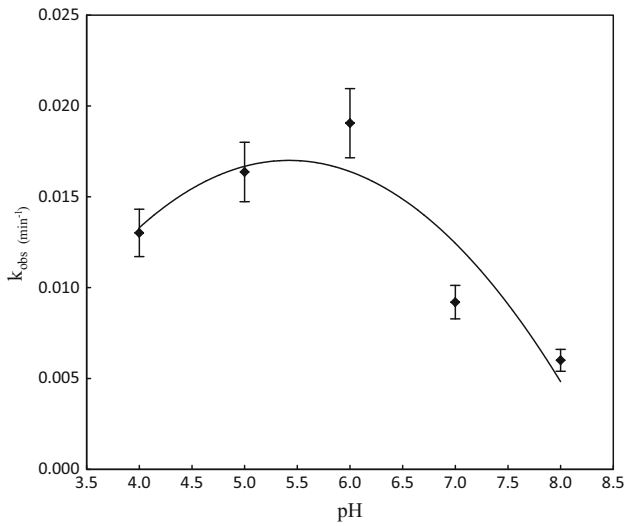

Fig. 11 Effect of pH on the rate constant of photo catalytic degradation of Bromothymol blue with Ru–TiO_2 at 25 °C, [Ru–TiO_2] = 100 mg l^{-1} [BTB] = 5 × 10^{-5} mol dm^{-3}

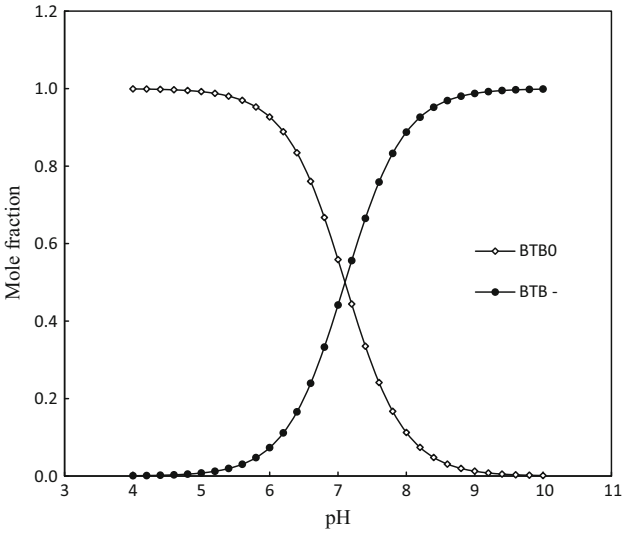

Fig. 12 Speciation of BTB at different pH

increases, the number of photons reaching the surface of photo-catalyst (Ru–TiO_2) also increases, consequently, increasing the number of electron–hole pairs. The holes decompose the BTB molecules adsorbed on the surface of Ru–TiO_2 particles and oxidize it to water resulting in their efficient degradation [10].

3.8 The mechanism of photo-catalytic degradation of BTB with Ru–TiO_2

When UV light was allowed fall on the photo-catalyst, electrons in the valence band were to the conduction band. Consequently, an electron–hole-pair is generated [47].

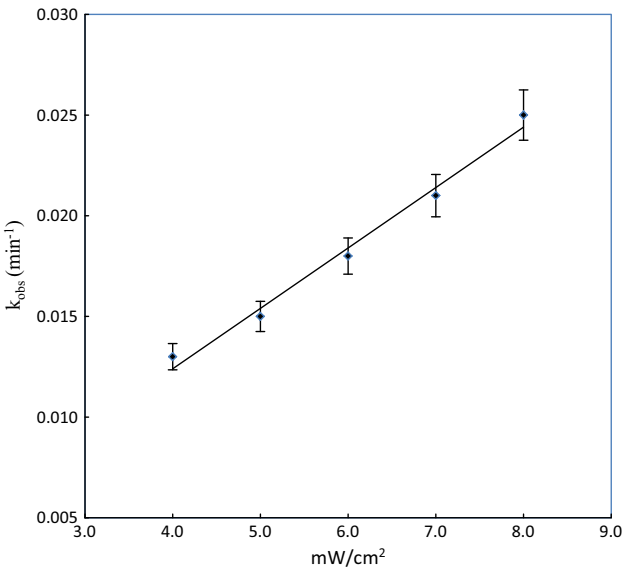

Fig. 13 BTB degradation under different UV intensities Bromothymol blue with Ru–TiO_2 at 25 °C, [Ru–TiO_2] = 100 mg l^{-1} [BTB] = 5 × 10^{-5} mol dm^{-3}

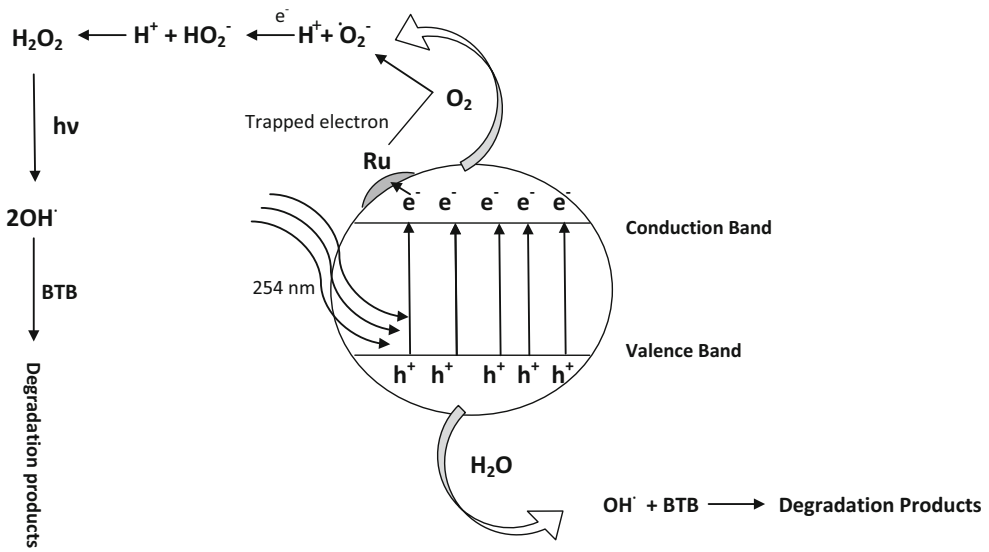

Fig. 14 Mechanism of photo catalytic degradation of BTB with Ru–TiO_2

$$Ru - TiO_2 + h\nu \rightarrow e^-_{cb} + h^+_{vb}$$

Here e^-_{cb} represents electrons in the conduction band and h^+_{vb} represents the holes in the valence band. The positive hole of the valence band reacts with a water molecule to produce hydroxide free radicals, where the superoxide anion radical is formed as a result of oxygen reduction by transfer of trapped electrons from Ru metal to oxygen as shown in Fig. 14 [48].

$$H_2O + h^+_{vb} \rightarrow {}^{\cdot}OH + H^+$$

$$O_2 + e^-_{cb} \rightarrow O_2^-$$

The above reaction eliminates the possibility of electron–hole recombination. The $^{\cdot}OH$ and $O_2{}^-$ produced in the above manner can then react with the BTB to yield degradation products.

$$O_2^{-\cdot} + H^+ \rightarrow HO_2^{\cdot}$$

$$H_2O_2 \rightarrow 2\ {}^{\cdot}OH$$

$$^{\cdot}OH + BTB \rightarrow \text{Degraded products}$$

$$BTB + e^-_{cb} \rightarrow \text{Degraded products}$$

It may be noted that all these reactions in photo-catalysis are possible due to the presence of both dissolved oxygen and water molecules. Without the presence of water molecules, the high hydroxyl radicals ($^{\cdot}OH$) could not be formed and inhibit the photo-catalytic degradation of liquid phase organic molecules.

4 Conclusions

The experimental results lead to following conclusions:

- Liquid impregnation method was used to synthesize Ru–TiO_2 nanoparticles.
- The particle size of TiO_2 decreases with increasing percentage of ruthenium doping.
- 0.8 % Ru–TiO_2 nanoparticles exhibited a better potential compared to UV and UV/TiO_2 techniques for the effective photo-catalytic degradation of bromothymol blue in acidic medium (pH 4–6).
- Photo-catalytic degradation of Bromothymol blue could be achieved in 100 min with 100 mg l^{-1} dosage of 0.8 % Ru–TiO_2.

References

1. S.A. Hosseini, P. Moalemzade, J. Mater. Sci. Mater. Electron. **27**, 8802–8806 (2016)
2. O.E. Ligrini, A. Oliveros, A.M. Braun, Chem. Rev. **93**, 671–698 (1993)
3. N.S. Arul, D. Mangalaraj, P.C. Chen, N. Ponpandian, P. Meena, Y. Masuda, J. Sol-Gel Sci. Technol. **64**, 515 (2012)
4. S.K. Kansal, P. Kundu, S. Sood, R. Lamba, A. Umar, S.K. Mehta, New J. Chem. **38**, 3220 (2014)
5. D. Chen, Z. Jiang, J. Geng, Q. Wang, D. Yang, Ind. Eng. Chem. Res. **46**, 2741 (2007)
6. Q. Sun, Y. Xu, J. Phys. Chem. C **114**, 18911 (2010)
7. M.M. Momeni, M. Mirhosseini, Z. Nazari, A. Kazempour, M. Hakimiyan, J. Mater. Sci. Mater. Electron. **27**, 8131–8137 (2016)
8. T. Kudo, Y. Kudo, A. Ruike, Catal. Today **122**, 14–19 (2007)
9. G. Zayani, L. Bousselmi, F. Mhenni, A. Ghrabi, Desalination **248**, 23–31 (2009)
10. U.I. Gaya, A.H. Abdullah, J. Photochem. Photobiol. C **9**, 1–12 (2008)
11. M. Mousavi-Kamazani, M. Salavati-Niasari, M. Sadeghinia, Mater. Lett. **142**, 145–149 (2015)
12. M. Panahi-Kalamuei, M. Mousavi-Kamazani, M. Salavati-Niasari, S.M. Hosseinpour-Mashkani, Ultrason. Sonochem. **23**, 246–256 (2015)

13. J. Li, L. Yan, Y. Wang, Y. Kang, C. Wang, S. Yang, J. Mater. Sci. Mater. Electron. **27**, 7834–7838 (2016)
14. A. Taicheng, H. Yang, W. Song, G. Li, H. Luo, J.C. William, J. Phys. Chem. A **114**, 2569–2575 (2010)
15. Z. Zarghami, M. Maddahfar, M. Ramezani, J. Mater. Sci. Mater. Electron. **26**, 6339–6343 (2015)
16. X. Jiang, Z. Li, Q. Lin, K. Dong, Y. Zhang, Z. Sun, J. Mater. Sci. Mater. Electron. **27**, 8856–8861 (2016)
17. L. Man, S.H. Seong, M. Mohseni, J. Mol. Catal. A **242**, 135–140 (2005)
18. X. Shu, J. He, D. Chen, Ind. Eng. Chem. Res. **47**, 4750–4753 (2005)
19. P. Govindhan, C. Pragathiswaran, J. Mater. Sci. Mater. Electron. **27**, 8778–8785 (2016)
20. L. Kumaresan, M. Mahalakshmi, M. Palanichamy, V. Murugesan, Ind. Eng. Chem. Res. **49**, 1480–1485 (2010)
21. N. Sasirekha, S.J.S. Basha, K. Shanti, Appl. Catal. B Environ. **62**, 169–180 (2006)
22. S.G. Ansari, F. Tuz-Zehra, H. Fouad, A.S. Hassenein, Z.A. Ansari, J. Mater. Sci. Mater. Electron. **26**, 5170–5174 (2015)
23. S.I. Shah, W. Li, C.P. Huang, O. Jung, C. Ni, Proc. Natl. Acad. Sci. USA PNAS **99**, 6482–6486 (2002)
24. M.M. Haque, M. Muneer, Dyes Pigments **75**, 443–448 (2007)
25. J. Choi, H. Park, M.R. Hoffmann, J. Phys. Chem. C **114**(2), 783–792 (2009)
26. K. Wetchakun, N. Wetchakun, S. Phanichphant, Adv. Mater. Res. **55–57**, 853–856 (2008)
27. V. Marinova, S.H. Lin, K.Y. Hsu, M.L. Hsieh, M.M. Gospodinov, V. Sainov, J. Mater. Sci. Mater. Electron. **14**, 857–858 (2003)
28. S. Ozkan, M.W. Kumthekar, G. Karakas, Catal. Today **40**, 3–14 (1998)
29. T. An, H. Yang, W. Song, G. Li, H. Luo, W.J. Cooper, J. Phys. Chem. A **114**(7), 2569–2575 (2010)
30. M.S. Lee, S.S. Hong, M. Mohseni, J. Mol. Catal. A **242**(1–2), 135–140 (2005)
31. A.N. Kadam, R.S. Dhabbe, M.R. Kokate, Y.B. Gaikwad, K.M. Garadkar, Spectrochim. Acta A Mol. Biomol. Spectrosc. **133**, 669–676 (2014)
32. S. Ullah, E.P. Ferreira-Neto, A.A. Pasa, C.C.J. Alcantara, J.J.S. Acuna, S.A. Bilmes, M.L.M. Ricci, R. Landers, T.Z. Fermino, U.P. Rodrigues-Filho, Appl. Catal. B Environ. **179**, 333–343 (2015)
33. D. Williams, C. Carter, *Transmission electron microscopy: a textbook for material science* (Springer, New York, 2009), p. 35
34. M.M. Ba-Abbad, A.H. Kadhum, A.B. Mohamad, M.S. Takriff, K. Sopian, Int. J. Electrochem. Sci. **7**, 4871–4888 (2012)
35. M. Hema, A. Yelil Arasi, P. Tamilselvi, R. Anbarasan, Chem. Sci. Trans. **2**(1), 239–245 (2013)
36. L. Liu, S. Chen, W. Sun, J. Xin, J. Mol. Struct. **1001**, 23–28 (2011)
37. C.N. Xu, J. Tamaki, N. Miura, N. Yamazoe, Sens. Actuators B Chem. **3**, 147–155 (1991)
38. B.K. Min, S.D. Choi, Sens. Actuators B Chem. **108**, 119–124 (2005)
39. G. Neri, A. Bonavita, G. Micali, N. Donato, F.A. Deorsola, P. Mossino, I. Amato, B. de Benedetti, Sens. Actuators B Chem. **117**, 196–204 (2006)
40. N.L. Wu, S.Y. Wang, I.A. Rusakova, Science **285**, 1375–1377 (1999)
41. M.M. Haque, M. Muneer, J. Environ. Manag. **69**, 169–176 (2003)
42. M. Qamar, M. Saquib, Desalination **171**, 185–193 (2004)
43. H. Chun, W. Yizhong, T. Hongxiao, Chemosphere **41**, 1205–1209 (2000)
44. C. Hu, Y. Tang, J.C. Yu, P.K. Wong, Appl. Catal. B Environ. **40**, 131–140 (2003)
45. E. Klotz, R. Doyle, E. Gross, B.J. Mattson, J. Chem. Educ. **88**, 637–639 (2011)
46. A. Verma, M. Sheoran, A.P. Toor, Indian J. Chem. Technol. **20**, 46–51 (2013)
47. I.K. Konstantinou, T.A. Albanis, Appl. Catal. B Environ. **49**, 1–14 (2004)
48. N.M. Mahmoodi, M. Arami, N.Y. Limaee, N.S. Tabrizi, J. Colloid, Interface Sci. **295**, 159–164 (2006)